Two-photon absorption towards pulse modulation in mechanically exfoliated and CVD monolayer cascaded MoS_2 structures

Yafeng Xie (谢亚锋)[1,2], Saifeng Zhang (张赛锋)[1,], Xiaoyan Zhang (张晓艳)[1], Ningning Dong (董宁宁)[1], Ivan M. Kislyakov[1], Song Luo (罗 松)[3], Zhanghai Chen (陈张海)[3], Jean-Michel Nunzi[1,4], Long Zhang (张 龙)[1], and Jun Wang (王 俊)[1,5,*]**

[1]*Laboratory of Micro-Nano Photonic and Optoelectronic Materials and Devices, Key Laboratory of Materials for High-Power Laser, Shanghai Institute of Optics and Fine Mechanics, Chinese Academy of Sciences, Shanghai 201800, China*

[2]*Center of Materials Science and Optoelectronics Engineering, University of Chinese Academy of Sciences, Beijing 100049, China*

[3]*State Key Laboratory of Surface Physics, Key Laboratory of Micro and Nano Photonic Structures of Ministry of Education, Department of Physics, Collaborative Innovation Center of Advanced Microstructures, Fudan University, Shanghai 200433, China*

[4]*Department of Physics, Engineering Physics & Astronomy and Department of Chemistry, Queen's University, Kingston K7L-3N6, Ontario, Canada*

[5]*State Key Laboratory of High Field Laser Physics, Shanghai Institute of Optics and Fine Mechanics, Chinese Academy of Sciences, Shanghai 201800, China*

**Corresponding author: jwang@siom.ac.cn; **corresponding author: sfzhang@siom.ac.cn*

Received March 13, 2019; accepted April 25, 2019; posted online July 16, 2019

Mechanical exfoliation (ME) and chemical vapor deposition (CVD) MoS_2 monolayers have been extensively studied, but the large differences of nonlinear optical performance between them have never been clarified. Here, we prepared MoS_2 monolayers using ME and CVD methods and investigated the two-photon absorption (TPA) response and its saturation. We found that the TPA coefficient of the ME monolayer was about $(1.88 \pm 0.21) \times 10^3$ cm/GW, nearly two times that of the CVD one at $(1.04 \pm 0.15) \times 10^3$ cm/GW. Furthermore, we simulated and compared the TPA-induced optical pulse modulation in multilayer cascaded structures, which is instructive and meaningful for the design of optical devices such as a beam shaper and optical limiter.

OCIS codes: 190.4400, 160.4236, 190.5970, 020.4180.
doi: 10.3788/COL201917.081901.

Atomically thin semiconducting transition metal dichalcogenides (TMDs) exhibit remarkable nonlinear optical (NLO) properties including layer-dependent second/third harmonic generation[1], two/multi-photon absorption[2–4], ultrafast saturable absorption[5–9], etc., which have been widely applied in two-dimensional (2D) photonics and optoelectronic devices[10–12]. Especially for 2D MoS_2, researchers have made great effort to prepare large area monolayer and few-layer films with distinct NLO properties using chemical vapor deposition (CVD), mechanical exfoliation (ME), and liquid phase exfoliation (LPE) methods. However, samples prepared by different methods show distinct optical performance. Taking second harmonic generation (SHG) as an example, the ME monolayer MoS_2 ($\chi^{(2)} \approx 10^{-7}$ m/V) exhibits a much stronger second-order NLO response than the CVD one ($\chi^{(2)} \approx 10^{-9}$ m/V)[13,14]. In terms of nonlinear absorption, the ME MoS_2 is greatly different from the CVD and LPE ones, which is reflected in practical mode-locking and Q-switching devices[15–17]. As a result, it is crucial for optical device applications to reveal the intrinsic optical properties of 2D TMDs prepared by different methods.

As is well known, in the TMDs MX_2 (M = Mo and W; X = S, Se, and Te), various types of defects, e.g., X vacancy, X interstitial, M vacancy, M interstitial, and MX and XX double vacancies, have been considered[18–20]. However, it still remains obscure how the defects affect the NLO properties of as-prepared MoS_2 nanosheets.

Here, we choose CVD and ME MoS_2 monolayers, typical TMDs with superior NLO properties, and make a comparative study of two-photon absorption (TPA) using a modified micro-intensity scan system. We found that the TPA coefficients of the two samples differed by nearly two times, which is ascribed to the large difference of the defect concentration between them[18–21]. In view of the huge advantages of MoS_2 in applications of pulse shaping and optical limiting due to its giant TPA coefficient, we simulated and compared the TPA-induced pulse modulation between CVD and ME monolayer cascaded structures.

Monolayer MoS_2 nanosheets were prepared onto transparent quartz using ME from natural crystal[22] and the CVD method[23], respectively. All of these samples were preliminarily identified by the optical microscope. As shown in Figs. 1(a) and 1(c), the side length of the samples

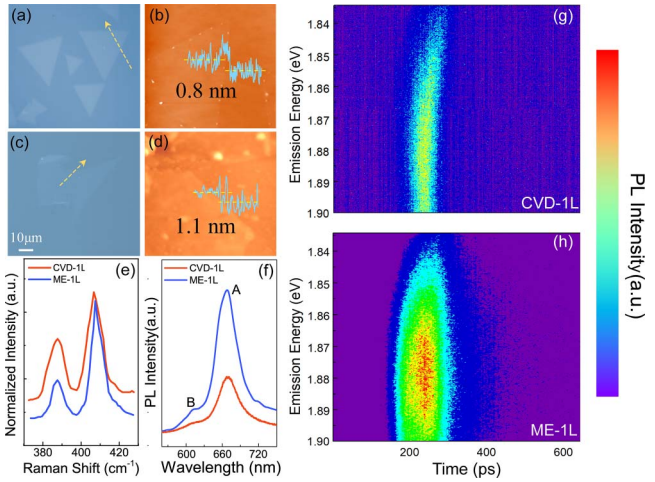

Fig. 1. (a)–(d) Optical microscope and AFM characterization of both CVD and ME MoS_2 monolayers. (e) Raman spectra imply that there are more defects in the CVD MoS_2 monolayer than in the ME one. (f) Steady PL spectra were measured, and strong PL quenching was observed in the CVD monolayer. (g), (h) The PL lifetime of an exciton in CVD and ME monolayers was measured using a streak camera.

was determined to be ~50 μm. The thickness and surface morphology were measured using atomic force microscopy (AFM), as shown in Figs. 1(b) and 1(d). The thickness of the ME monolayer is ~1.1 nm and is slightly larger than that in general, which should be caused by the air gap between the sample and the substrate, while the thickness of the CVD monolayer is ~0.7 nm.

Raman spectroscopy has been identified as a convincing tool to determine the crystal structure of 2D MoS_2 nanosheets[24,25]. In this work, Raman spectroscopy measurements were conducted by using a confocal microscopy system combining a diode laser at 532 nm. The Raman peak interval between two active vibration modes, E^1_{2g} and A_{1g}, is ~17.99 cm^{-1} and ~19.87 cm^{-1} for CVD and ME monolayers, respectively. Figure 1(e) shows the broadening of two Raman peaks in the CVD monolayer, indicating that defects have made an impact on the crystal structure[26,27]. In addition, the two Raman vibration modes give a strong proof that all the samples used in our work are 2H-MoS_2[28].

Under the same excitation, we acquired the steady photoluminescence (PL) spectra of ME and CVD monolayer MoS_2. It is obvious that the ME monolayer exhibited much stronger PL intensity than the CVD one, as shown in Fig. 1(f). The PL quenching in the CVD monolayer indicates that the defect-assisted non-radiative transition plays an important role in it[29]. In addition, the PL lifetime was measured using a streak camera (Optronis). The samples were excited by the ultrafast laser with the pulse width of 120 fs at the wavelength of 600 nm and repetition rate of 80 MHz. As Figs. 1(g) and 1(h) show, the CVD monolayer exhibited much faster and weaker excitonic emission than the ME one, which is exponentially fitted (Supplementary Information Fig. S1). It can be ascribed to stronger defect-assisted Auger scattering, leading to fast exciton annihilation and non-radiative electron-hole recombination[30].

In this work, TPA processes in monolayer MoS_2 were investigated at room temperature (~300 K) with a modified micro-intensity scan system, as illustrated in Fig. 2[3,31]. The 350 fs laser pulses at 1030 nm (~1.2 eV) were generated from a mode-locked fiber laser (1 kHz) and attenuated with an electrically tunable neutral density filter. The laser beam was finally focused with a waist radius ω_0 of ~5 μm on the surface of MoS_2 using an $f/35$ mm lens. Herein, the excitation source with photon energy of 1.2 eV was chosen to generate good resonant interaction with monolayer MoS_2 through a distinct two-photon process due to the existence of dark excitonic states[31–33].

Here, the absorption process can be analyzed using the propagation equation[34,35]:

$$\frac{\mathrm{d}I(z)}{\mathrm{d}z} = -\alpha I - \beta(I) I^2(z), \tag{1}$$

where z is the propagation distance in the sample. α is the coefficient of one-photon absorption, which is negligible owing to the smaller value of the photon energy of 1.2 eV than the optical bandgap. $\beta(I)$, the TPA coefficient, is dependent on the incident laser intensity. In our experiment, the excitation source was a series of Gaussian pulses in time and space, that is

$$I(r,t) = I_0 \cdot \exp(-2r^2/w_p^2) \cdot \exp(-t^2/\tau_0^2). \tag{2}$$

Here, w_p and τ_0 represent the radius of the pump beam waist and the half-pulse width, respectively.

The effective TPA coefficient can be obtained quantitatively using a homogeneously broadened two-band theory[36–38]:

$$\beta_{\mathrm{eff}}(I) = \frac{\beta_0}{1 + (I/I_{\mathrm{sat}})^2}, \tag{3}$$

where $\beta_0 = \sigma_{\mathrm{TPA}} \frac{g_2}{g_1} N_0$, N_0 is the concentration of the absorber (i.e., MoS_2 molecular density, in cm^{-3}). In an ideal monolayer MoS_2 crystal, N_0 is estimated to be $\sim 1.8 \times 10^{22}$ cm^{-3}. σ_{TPA} is the TPA cross section, g_2 (g_1) is the electronic degeneracy of the upper (lower) state. The TPA-active excitons are sixfold degenerate, which corresponds to the three degenerate 2p states in a 2D

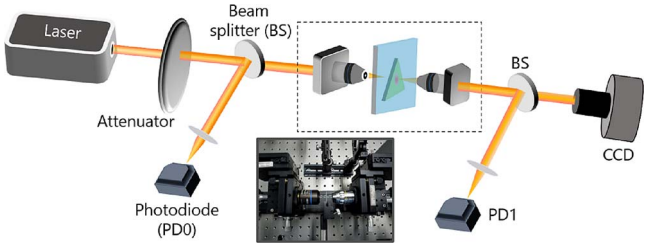

Fig. 2. Schematic diagram of the setup of the micro-intensity scan.

hydrogen model, multiplied by the two valleys of K and K' points in the Brillouin zone, so that $\frac{g_2}{g_1}$ equals six in Eq. (4)[39]. Based on the above theories, the TPA coefficients are acquired and shown in Fig. 3(c). The ME monolayer exhibits a much larger TPA coefficient of $(1.88 \pm 0.21) \times 10^3$ cm/GW than the CVD one of $(1.04 \pm 0.15) \times 10^3$ cm/GW. The TPA process in MoS_2 during the pulse duration time ($\tau_p = 350$ fs) is illustrated in Fig. 3(b), where an electron transits from the energy level E_0 to E_2 via absorbing two degenerate photons instantaneously. According to the selection rule, E_2 represents the 2p dark excitonic state here. Then, the excited excitons relax to E_1 through an electron–electron scattering process in less than 60 fs[40,41]. The detailed carrier dynamics of the TPA process are simulated in the Supplementary Information and schematically shown in Fig. S2. The mid-gap defect states will decrease the TPA coefficients, as defect-induced one-photon absorption in the CVD monolayer may play a role[21].

The saturation intensity $I_{\rm sat}$ obtained in the micro-intensity scan experiment based on Eqs. (1) and (3), as shown in the inset of Fig. 3(c), can be deduced theoretically. In the homogeneously broadened model, the saturation intensity can be expressed as[36,37]

$$I_{\rm sat} = \sqrt{\frac{2\hbar\omega}{\tau_{\rm p}\sigma_{\rm TPA}\left(1+\frac{g_2}{g_1}\right)}}, \tag{4}$$

where $\tau_{\rm p}$ is the full width at half-maximum of the femtosecond laser pulse ($\tau_{\rm p} = 350$ fs). Therefore, with the TPA cross section $\sigma_{\rm TPA}$ obtained from $\sigma_{\rm TPA} = \frac{\beta_0}{N_0}\frac{g_1}{g_2}$, the saturation intensity of ME monolayer MoS_2 can be calculated as ~128 GW/cm^2, while the value of our experimental fitting result is ~146 GW/cm^2 according to Eqs. (1) and (3). Likewise, the calculated value for $I_{\rm sat}$ of the CVD-grown monolayer is ~172 GW/cm^2, which is comparable with the fitting value of ~217 GW/cm^2. The estimation of the saturation intensity is in the same order of magnitude with the experimental fitting results for both CVD and ME monolayers, implying that our fitting is reasonable. The saturation intensity of TPA is larger than that of monolayer WS_2 (~26 GW/cm^2)[2]. Our results indicate that it is more difficult for CVD monolayer MoS_2 to be saturated in the TPA process than the ME one.

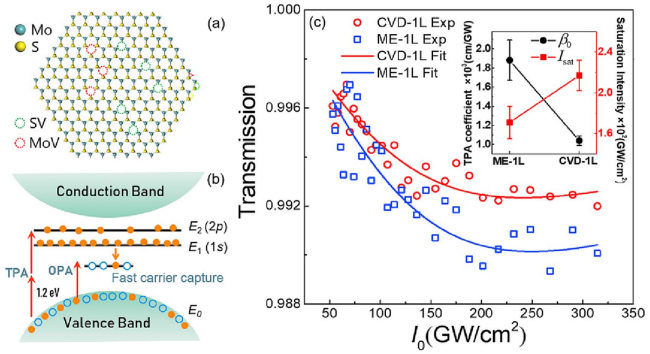

Fig. 3. (a) Schematic structures of monolayer MoS_2 and vacancies in it. SV, sulfur vacancy; MoV, molybdenum vacancy. (b) Energy levels in CVD and ME MoS_2, optical transition, and defect-induced fast carrier capture processes (TPA, two-photon absorption; OPA, one-photon absorption). (c) Nonlinear transmittance versus incident pulse peak irradiance for MoS_2 monolayers. The solid lines are the fitting results obtained by numerically solving Eq. (1). Inset: the values of the TPA coefficient and corresponding saturation intensity.

The TPA coefficient of monolayer MoS_2 is 3–4 orders of magnitude larger than those of many common semiconductors like ZnO and GaAs[42,43]. In view of this giant advantage, it possesses great potential in optical pulse modulation and optical limiting applications. Therefore, it is necessary and interesting to examine the difference between CVD and ME MoS_2. In this part, we simulated how the TPA saturation effect modulates the optical pulse in CVD and ME monolayers and made a comparison with a cascaded multilayer structure.

The spatial intensity distribution of the femtosecond pulses we used is of a Gaussian profile with a waist radius of $\omega_0 \approx 5$ μm, the same as the experiment. Considering that the value of β changes with pulse intensity according to the homogeneously broadened model, the TPA coefficient will not be a constant in the radial direction of a laser spot. This means that the differential transmission intensity $\Delta I/I_0$ at different radial positions in the spot will change. The differential intensity reflects the spatial modulation ability of the MoS_2 nanofilms. However, the ultrashort interaction length in the monolayer is detrimental to the modulator design. As a result, a simple solution to this problem is having a series of cascading MoS_2 monolayers[44], and the simulated results are demonstrated in Fig. 4. Figure 4(a) depicts the resulting $\Delta I/I_0$ distribution when a pulse passes through the 1L, 50L, and 100L CVD and ME MoS_2, respectively, under the same excitation of 300 GW/cm^2. We can see that in the CVD 1L case, the TPA saturation effect is not large enough, and the central area shows an intensive absorption. But, in the ME 1L case, the TPA is remarkably saturated, and the absorption decreases, which results in the darker spot in Fig. 4(a). In a cascaded structure, the transmitted intensity decreases layer by layer, making the TPA saturation insignificant. Therefore, a more uniform absorption can be seen in the multilayer systems, and the largest pulse intensity differential will move from the margin of the spot to the center. From Fig. 4(b), it can be seen that the stronger TPA effect in the ME cascaded structure results in greater pulse modulation amplitude with the increasing of layers. Furthermore, Fig. 4(c) shows the optical limiting performance of both CVD and ME cascaded structures, which directly reveals the difference of these two systems. In conclusion, according to the simulation results, due to larger TPA coefficient, the ME MoS_2 monolayer and the cascaded structure exhibit better optical pulse modulation and optical limiting performance compared to CVD ones.

In summary, monolayer MoS_2 nanosheets have been prepared by ME and CVD methods. We studied the

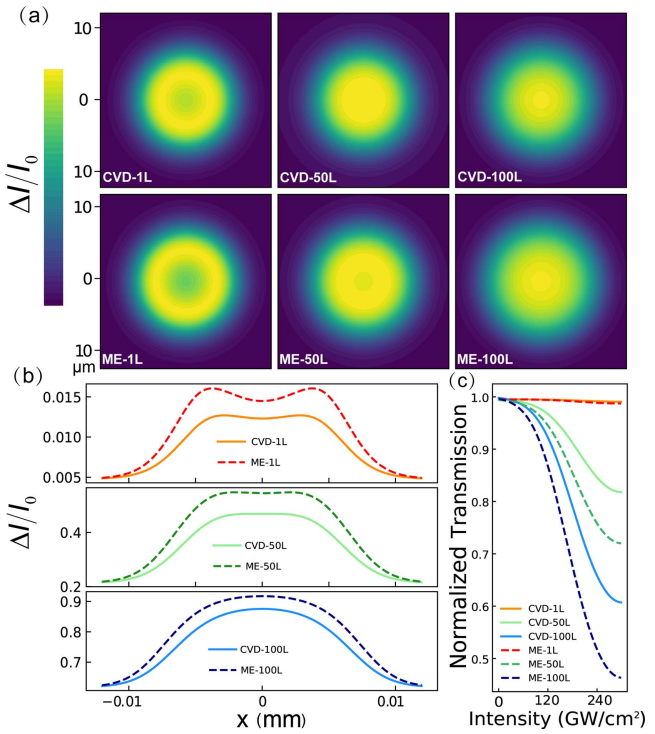

Fig. 4. (a), (b) Differential intensity ($\Delta I/I_0$) distribution of the output pulse under the same excitation intensity of 300 GW/cm^2 in 1L, 50L, and 100L CVD and ME MoS_2, respectively. (c) Optical limiting performance.

difference of the degenerate TPA effect between them. The TPA coefficient of the CVD monolayer is only about one half of that of the ME one, mainly due to the one-photon absorption induced by mid-gap defect states. Furthermore, we simulated and compared the pulse modulation performance between CVD and ME cascaded monolayer structures. It can provide meaningful guides for the design of optical devices like a beam shaper and optical limiters.

This work was supported by the National Natural Science Foundation of China (NSFC) (Nos. 61675217 and 11874370), the Strategic Priority Research Program of CAS (No. XDB16030700), the Key Research Program of Frontier Science of CAS (No. QYZDB-SSW-JSC041), the Program of Shanghai Academic Research Leader (No. 17XD1403900), the Natural Science Foundation of Shanghai (No. 18ZR1444700), the Shanghai Rising-Star Program (A Type 19QA1410000), and the Youth Innovation Promotion Association, CAS.

References

1. Y. H. Tang, K. C. Mandal, J. A. McGuire, and C. W. Lai, Phys. Rev. B **94**, 125302 (2016).
2. S. F. Zhang, N. N. Dong, N. McEvoy, M. O'Brien, S. Winters, N. C. Berner, C. Yim, Y. X. Li, X. Y. Zhang, Z. H. Chen, L. Zhang, G. S. Duesberg, and J. Wang, ACS Nano **9**, 7142 (2015).
3. Y. Li, N. Dong, S. Zhang, X. Zhang, Y. Feng, K. Wang, L. Zhang, and J. Wang, Laser Photon. Rev. **9**, 427 (2015).
4. F. Zhou and W. Ji, Laser Photon. Rev. **11**, 1700021 (2017).
5. K. P. Wang, J. Wang, J. T. Fan, M. Lotya, A. O'Neill, D. Fox, Y. Y. Feng, X. Y. Zhang, B. X. Jiang, Q. Z. Zhao, H. Z. Zhang, J. N. Coleman, L. Zhang, and W. J. Blau, ACS Nano **7**, 9260 (2013).
6. H. Zhang, S. B. Lu, J. Zheng, J. Du, S. C. Wen, D. Y. Tang, and K. P. Loh, Opt. Express **22**, 7249 (2014).
7. J. Zhang, H. Ouyang, X. Zheng, J. You, R. Z. Chen, T. Zhou, Y. Z. Sui, Y. Liu, X. G. Cheng, and T. Jiang, Opt. Lett. **43**, 243 (2018).
8. T. Jiang, R. L. Miao, J. Zhao, Z. J. Xu, T. Zhou, K. Wei, J. You, X. Zheng, Z. Y. Wang, and X. Cheng, Chin. Opt. Lett. **17**, 020005 (2019).
9. X. F. Xin, F. Liu, X. Q. Yan, W. W. Hui, X. Zhao, X. G. Gao, Z. B. Liu, and J. G. Tian, Opt. Express **26**, 33895 (2018).
10. Z. P. Sun, A. Martinez, and F. Wang, Nat. Photon. **10**, 227 (2016).
11. Z. Yin, H. Li, H. Li, L. Jiang, Y. Shi, Y. Sun, G. Lu, Q. Zhang, X. Chen, and H. Zhang, ACS Nano **6**, 74 (2012).
12. H. S. Lee, S. W. Min, Y. G. Chang, M. K. Park, T. Nam, H. Kim, J. H. Kim, S. Ryu, and S. Im, Nano Lett. **12**, 3695 (2012).
13. N. Kumar, S. Najmaei, Q. Cui, F. Ceballos, P. M. Ajayan, J. Lou, and H. Zhao, Phys. Rev. B **87**, 161403 (2013).
14. D. J. Clark, V. Senthilkumar, C. T. Le, D. L. Weerawarne, B. Shim, J. I. Jang, J. H. Shim, J. Cho, Y. Sim, M. J. Seong, S. H. Rhim, A. J. Freeman, K. H. Chung, and Y. S. Kim, Phys. Rev. B **90**, 121409 (2014).
15. H. D. Xia, H. P. Li, C. Y. Lan, C. Li, X. X. Zhang, S. J. Zhang, and Y. Liu, Opt. Express **22**, 17341 (2014).
16. J. Lu, X. Zou, C. Li, W. K. Li, Z. Z. Liu, Y. Q. Liu, and Y. X. Leng, Chin. Opt. Lett. **15**, 041401 (2017).
17. E. J. Aiub, D. Steinberg, E. A. Thoroh De Souza, and L. A. M. Saito, Opt. Express **25**, 10546 (2017).
18. J. Hong, Z. Hu, M. Probert, K. Li, D. Lv, X. Yang, L. Gu, N. Mao, Q. Feng, L. Xie, J. Zhang, D. Wu, Z. Zhang, C. Jin, W. Ji, X. Zhang, J. Yuan, and Z. Zhang, Nat. Commun. **6**, 6293 (2015).
19. Y. Lee and J. Kim, ACS Photon. **5**, 4187 (2018).
20. S. Haldar, H. Vovusha, M. K. Yadav, O. Eriksson, and B. Sanyal, Phys. Rev. B **92**, 235408 (2015).
21. X. Zhang, S. Zhang, Y. Xie, J. Huang, L. Wang, Y. Cui, and J. Wang, Nanoscale **10**, 17924 (2018).
22. K. S. Novoselov, A. K. Geim, S. V. Morozov, D. Jiang, Y. Zhang, S. V. Dubonos, I. V. Grigorieva, and A. A. Firsov, Science **306**, 666 (2004).
23. Y. H. Lee, X. Q. Zhang, W. Zhang, M. T. Chang, C. T. Lin, K. D. Chang, Y. C. Yu, J. T. Wang, C. S. Chang, L. J. Li, and T. W. Lin, Adv. Mater. **24**, 2320 (2012).
24. H. Li, Q. Zhang, C. C. R. Yap, B. K. Tay, T. H. T. Edwin, A. Olivier, and D. Baillargeat, Adv. Funct. Mater. **22**, 1385 (2012).
25. X. L. Li, W. P. Han, J. B. Wu, X. F. Qiao, J. Zhang, and P. H. Tan, Adv. Funct. Mater. **27**, 1604468 (2017).
26. S. Tongay, J. Suh, C. Ataca, W. Fan, A. Luce, J. S. Kang, J. Liu, C. Ko, R. Raghunathanan, J. Zhou, F. Ogletree, J. Li, J. C. Grossman, and J. Wu, Sci. Rep. **3**, 2657 (2013).
27. H. Li, C. Tsai, A. L. Koh, L. Cai, A. W. Contryman, A. H. Fragapane, J. H. Zhao, H. S. Han, H. C. Manoharan, F. Abild-Pedersen, J. K. Norskov, and X. L. Zheng, Nat. Mater. **15**, 364 (2016).
28. C. Lee, H. Yan, L. E. Brus, T. F. Heinz, J. Hone, and S. Ryu, ACS Nano **4**, 2695 (2010).
29. H. Wang, J. H. Strait, C. Zhang, W. Chan, C. Manolatou, S. Tiwari, and F. Rana, Phys. Rev. B **91**, 165411 (2015).
30. N. Kumar, Q. Cui, F. Ceballos, D. He, Y. Wang, and H. Zhao, Phys. Rev. B **89**, 125427 (2014).
31. F. Zhou and W. Ji, Opt. Lett. **42**, 3113 (2017).
32. D. Y. Qiu, F. H. da Jornada, and S. G. Louie, Phys. Rev. Lett. **111**, 216805 (2013).
33. F. Zhou, J. H. Kua, S. Lu, and W. Ji, Opt. Express **26**, 16093 (2018).

34. B. Taheri, H. Liu, B. Jassemnejad, D. Appling, R. C. Powell, and J. J. Song, Appl. Phys. Lett. **68**, 1317 (1996).
35. G. S. He, Q. D. Zheng, A. Baev, and P. N. Prasad, J. Appl. Phys. **101**, 083108 (2007).
36. S. M. Kirkpatrick, R. R. Naik, and M. O. Stone, J. Phys. Chem. B **105**, 2867 (2001).
37. J. He, J. Mi, H. P. Li, and W. Ji, J. Phys. Chem. B **109**, 19184 (2005).
38. N. N. Dong, Y. X. Li, S. F. Zhang, N. McEvoy, R. Gatensby, G. S. Duesberg, and J. Wang, ACS Photon. **5**, 1558 (2018).
39. F. Wu, F. Qu, and A. H. MacDonald, Phys. Rev. B **91**, 075310 (2015).
40. A. Tanaka, N. J. Watkins, and Y. Gao, Phys. Rev. B **67**, 113315 (2003).
41. H. Shi, R. Yan, S. Bertolazzi, J. Brivio, B. Gao, A. Kis, D. Jena, H. G. Xing, and L. Huang, ACS Nano **7**, 1072 (2013).
42. E. W. V. Stryland, M. A. Woodall, H. Vanherzeele, and M. J. Soileau, Opt. Lett. **10**, 490 (1985).
43. D. Huang, J. I. Chyi, and H. Morkoç, Phys. Rev. B **42**, 5147 (1990).
44. W. Chen, G. Wang, S. Qin, C. Wang, J. Fang, J. Qi, X. Zhang, L. Wang, H. Jia, and S. Chang, AIP Adv. **3**, 042123 (2013).